

Five-fold Precision Enhancement in a Cold Atom Experiment via Adaptive Symmetry-Informed Bayesian Strategies

Matt Overton,^{1,*} Jesús Rubio,^{2,*} Nathan Cooper,¹ Daniele Baldolini,¹
David Johnson,¹ Janet Anders,^{3,4} and Lucia Hackermüller¹

¹*School of Physics and Astronomy, University of Nottingham,
University Park, Nottingham NG7 2RD, United Kingdom*

²*School of Mathematics and Physics, University of Surrey, Guildford GU2 7XH, United Kingdom*

³*Department of Physics and Astronomy, University of Exeter, Stocker Road, Exeter EX4 4QL, United Kingdom*

⁴*Institute of Physics and Astronomy, University of Potsdam, 14476 Potsdam, Germany*

(Dated: 7th November 2024)

Bayesian methods promise enhanced device performance and accelerated data collection. We demonstrate an adaptive Bayesian measurement strategy for atom number estimation in a quantum technology experiment, utilising a symmetry-informed loss function. Compared to a standard unoptimised strategy, our method yields a five-fold reduction in the fractional variance of the atom number estimate. Equivalently, it achieves the target precision with a third of the data points previously required. We provide general expressions for the optimal estimator and error for any quantity amenable to symmetry-informed strategies, facilitating the application of these strategies in quantum computing, communication, metrology, and the wider quantum technology sector.

From advances in gravitational wave detection [1, 2] to applications such as brain pattern imaging [3], magnetic sensing [4, 5] or inertial navigation [6], quantum technologies are revolutionising fundamental and applied research. Rapid estimation of platform parameters, as well as precise state preparation and control, underpins this success, enabling, e.g., efficient interferometric measurements [7, 8] and high-fidelity readout within a limited coherence time in quantum computing [9, 10]. Estimation efficiency is critical for advancing quantum technologies [4, 11] and for testing the fundamental laws of nature [12–16].

The most widely adopted framework for benchmarking and enhancing measurement processes is local estimation theory [17–20]. In this context, the rate of information acquisition is increased by optimising the Fisher information, a sensitivity metric [21, 22], over probe states and measurement operators. However, information loss can still incur at the data processing stage [23–28], thus slowing the estimation process, because, to achieve the promised sensitivity, one must also saturate the Cramér-Rao bound and this often requires an asymptotically large number of shots [17, 19].

Bayesian estimation theory offers a flexible alternative [21, 29]. Within this framework, optimality is established by minimising an uncertainty metric based on a probabilistic description of the experimental platform, enabling maximum information acquisition for any sample size or parameter range and thereby accelerating data collection. The effectiveness of Bayesian methods has been demonstrated within a small number of atomic, molecular, and optical experiments and was mainly considered for phase estimation [30–41]. The key to this success is the direct optimisation of individual measurements within a finite sequence. Yet, despite the clear advantages of the Bayesian approach and its well-established theoretical foundations [19, 21, 29, 42–46], experimental adoption remains limited, revealing a need for a clear and unified methodology for implementation.

In this Letter we present a systematic, symmetry-informed

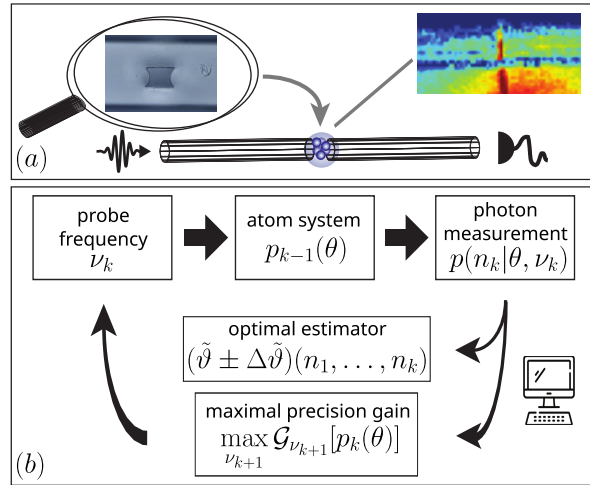


Figure 1. (a) Sketch of an ensemble of cold Cs atoms confined in a microscopic hole that intersects the core of an optical fibre. Atoms are probed via photon-counting detection of resonant light travelling along the fibre [47]. (b) Bayesian sensing using an adaptive, symmetry-informed strategy: the information gained about the atomic system from recorded photon-counts is used to yield a new optimal probe laser frequency offering maximum information gain from the next measurement shot. The precision gain is informed by the symmetries of the platform. The final estimate is sequentially improved as more photon-counts are recorded.

protocol for experimental Bayesian sensing applicable to parameters that are not phases, such as atom number, decay rate, or relative weight. By accounting for the symmetries of the object platform [29, 46], and using adaptive techniques [48–51], we propose a unified standard for optimal metrology, facilitating its adoption within the quantum technology sector and significantly expanding beyond conventional phase estimation. Its effectiveness is demonstrated through atom number estimation in a cold atom experiment (see Fig. 1.a) [47, 52]: a prototype for the integration of cold-atom based sensors,

memories and multi-qubit gates within existing photonic circuit architectures [53]. The proposed protocol yields a five-fold reduction in noise-to-signal ratio, or, equivalently, reduces the number of shots required to achieve the target precision to a third. This proves the protocol's utility in enabling faster, more precise estimation and demonstrates its practical applicability for rapid adoption in experiments.

Adaptive symmetry-informed strategies.—Finding efficient estimates amounts to solving an optimisation problem [21, 42, 50, 54]. We first present a general technique for optimal estimation and then apply it to atom number metrology. Derivations and examples are provided in the Supplemental Material.

Let $\theta \in [\theta_{\min}, \theta_{\max}]$ be a hypothesis for an unknown parameter Θ to be determined indirectly through a measurement with outcome n . A prior probability $p(\theta)$ encodes the initial information and is *updated* via Bayes's theorem as

$$p(\theta) \mapsto p(\theta|n, y) \propto p(\theta)p(n|\theta, y) \quad (1)$$

upon recording n . Here, $p(n|\theta, y)$ is a likelihood function relating n with θ and a control parameter y , while $p(\theta|n, y)$ is the posterior probability. When k outcomes $\mathbf{n} = (n_1, \dots, n_k)$ are measured using control parameters $\mathbf{y} = (y_1, \dots, y_k)$, the posterior

$$p(\theta|\mathbf{n}, \mathbf{y}) \propto p(\theta) \prod_{i=1}^k p(n_i|\theta, y_i) \quad (2)$$

contains all the information available about the true Θ [21, 35]. Once calculated, the estimator and uncertainty

$$\tilde{\vartheta}_{\mathbf{y},f}(\mathbf{n}) = f^{-1} \left[\int d\theta p(\theta|\mathbf{n}, \mathbf{y}) f(\theta) \right], \quad (3a)$$

$$\Delta \tilde{\vartheta}_{\mathbf{y},f}(\mathbf{n}) = \frac{\sqrt{\mathcal{L}_{\mathbf{y},f}(\mathbf{n})}}{|f'[\tilde{\vartheta}_{\mathbf{y},f}(\mathbf{n})]|} \quad (3b)$$

are *optimal* under quadratic losses [46]. Here, f is a free function and

$$\mathcal{L}_{\mathbf{y},f}(\mathbf{n}) = \int d\theta p(\theta|\mathbf{n}, \mathbf{y}) f(\theta)^2 - f[\tilde{\vartheta}_{\mathbf{y},f}(\mathbf{n})]^2 \quad (4)$$

is the information loss incurred by processing (\mathbf{n}, \mathbf{y}) .

Eqs. (3) enable experimental symmetry-informed estimation [46]. This provides maximum information for any parameter range or sample size by exploiting symmetries through the choice of f . For example, the likelihood may be invariant under a symmetry group [55], or we may enforce invariance under all reparametrisations [29]. More generally, parameter types can be associated with transformations such as translations for shifts or rescalings for rates [21, 56]. These symmetries determine maximum ignorance priors of the form [46, 55]

$$p_{\text{MI}}(\theta) \propto f'(\theta) \quad (5)$$

from which the function f required to use Eqs. (3) can be calculated.

Moreover, the information loss (4) can be adaptively reduced by selecting y_k for the k -th measurement to maximise the precision gain [35, 46]

$$\mathcal{G}_{y_k,f} = \sum_n p(n|y_k) f[\tilde{\vartheta}_{y_k,f}(n)]^2. \quad (6)$$

Here, $p(n|y_k) = \int d\theta p_{k-1}(\theta)p(n|\theta, y_k)$, with

$$p_{k-1}(\theta) := \begin{cases} p(\theta) & \text{if } k = 1 \\ p(\theta) \prod_{i=1}^{k-1} p(n_i|\theta, y_i) & \text{for } k > 1, \end{cases} \quad (7)$$

and $\tilde{\vartheta}_{y_k,f}(n)$ is defined as in Eq. (3a) using $p(\theta|n, y_k) \propto p_{k-1}(\theta)p(n|\theta, y_k)$.

Eqs. (3) and (6) constitute our first result. As we shall see next, they enable the experimental implementation of optimal estimators for any parameter for which a suitable f exists.

Atom number metrology.—In the experiment analysed here [47], determining the number of atoms required 30 – 100 shots per estimate, rendering atom number estimation the main rate-limiting step. This requirement is typical and also occurs in atom-nanofibre experiments [57, 58], precision magnetometers [59] and atom interferometry [60]. The aim is to address this problem with an adaptive strategy based on Eq. (6) [Fig. 1.b] and an optimal atom number estimator $\tilde{N}_\nu(\mathbf{n}) \pm \Delta \tilde{N}_\nu(\mathbf{n})$ built upon Eqs. (3).

In this setup, near-resonant light propagating through a fibre is absorbed by the atoms in the intersection at a rate proportional to [47]

$$\zeta_\nu = \frac{\Gamma^2}{\Gamma^2 + 4(\nu - \nu_r)^2}, \quad (8)$$

where ν is the laser frequency, and Γ and ν_r are the natural linewidth and resonant frequency of the atomic transition, respectively. The frequency ν is used as a control parameter by allowing variation from ν_r . Since the light intensity is low compared to the saturation intensity of the atomic transition, the optical power propagating through the fibre is attenuated such that the expected photon count is

$$\bar{n}_\nu(\Phi, \Theta) = \Phi e^{-\zeta_\nu \Theta}. \quad (9)$$

Here, Φ is the expected photon number detected with no atoms present, $\exp(-\zeta_\nu \Theta)$ is the transmittance of the medium and Θ its on-resonance optical depth. Both Φ and Θ are initially unknown.

Given that ordinary (unsqueezed) light is Poissonian, the photon count statistics reads

$$p(n|\Phi, \Theta, \nu) = P[n|\bar{n}_\nu(\Phi, \Theta)], \quad (10)$$

where $P(n|z) = z^n e^{-z}/n!$. The number of atoms, N , is estimated by counting photons with and without atoms loaded into the intersection ($n = n_a$ and $n = n_b$, respectively). Since $N = \kappa \Theta$ [47], with constant κ , symmetry-informed estimation can be applied directly to the optical depth Θ [61, 62].

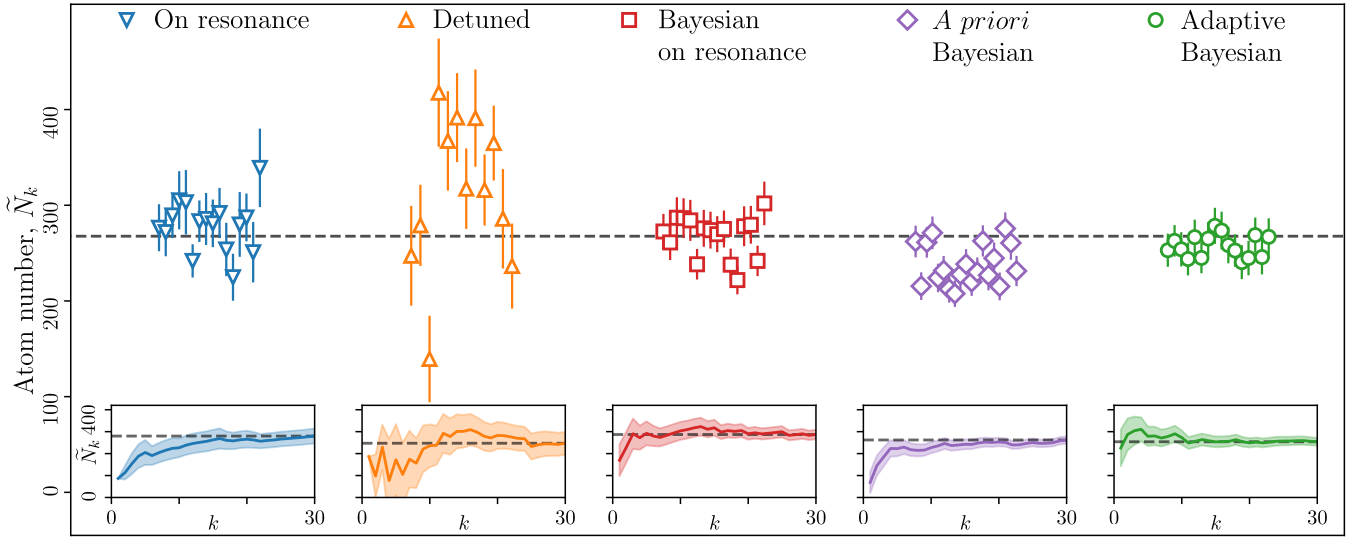


Figure 2. Atom number estimates resulting from measurements using the standard (blue and orange) and Bayesian estimation strategies (red, purple and green) described in the text. Each point estimate employs $k = 30$ measurement shots. In the on-resonance and detuned cases, error bars are given by the standard error for each 30-shot measurement, and via Eq. (14b) otherwise. The insets show the progression of the estimate with increasing k , for a single measurement run, in each case. The shading denotes the aforementioned errors. The small differences in the mean value obtained with each method are consistent with normal experimental drifts in loading efficiency, owing to the temporal separation of the data collection using each methodology. The dashed lines indicate final estimates in the insets and overall average across all methods in the main figure, shown here to guide the eye.

To use Eqs. (3), we need to select f exploiting symmetries in the system via Eq. (5), and this requires an ignorance prior. Let $\varphi \in [\varphi_{\min}, \varphi_{\max}]$ and $\theta \in [\theta_{\min}, \theta_{\max}]$ be the hypotheses for Φ and Θ , respectively. When two observers run the experiment at frequency ν , their average photon counts are comparable, but their initial hypotheses can differ due to prior ignorance. That is, $\bar{n}_\nu(\varphi', \theta') = \bar{n}_\nu(\varphi, \theta)$, so that $\varphi'/\varphi = \exp[\zeta_\nu(\theta' - \theta)]$. Equating both sides to a positive γ reveals transformations

$$\varphi' = \gamma\varphi, \quad \zeta_\nu\theta' = \zeta_\nu\theta + \log(\gamma) \quad (11)$$

under which Eq. (10) is invariant. Then, if both observers are equally ignorant, and given that ν does not inform Φ and Θ , their priors must respect the aforementioned invariance as $p_{\text{MI}}(\varphi', \theta')d\varphi'd\theta' = p_{\text{MI}}(\varphi, \theta)d\varphi d\theta$ [21]. As shown in the Supplemental Material, this leads to the multiparameter prior

$$p_{\text{MI}}(\varphi, \theta) = \left[(\theta_{\max} - \theta_{\min}) \log \left(\frac{\varphi_{\max}}{\varphi_{\min}} \right) \varphi \right]^{-1}. \quad (12)$$

Since only Θ is of interest, we further marginalise over Φ , i.e.,

$$p_{\text{MI}}(\theta) = \int_{\varphi_{\min}}^{\varphi_{\max}} d\varphi p_{\text{MI}}(\varphi, \theta) \propto 1. \quad (13)$$

Consequently, by combining Eqs. (5) and (13) to calculate f , and inserting this into Eqs. (3), we find the optimal atom num-

ber estimator and its uncertainty

$$\tilde{N}_\nu(\mathbf{n}) = \kappa \int_{\theta_{\min}}^{\theta_{\max}} d\theta p(\theta|\mathbf{n}, \nu)\theta, \quad (14a)$$

$$\Delta\tilde{N}_\nu(\mathbf{n})^2 = \kappa^2 \int_{\theta_{\min}}^{\theta_{\max}} d\theta p(\theta|\mathbf{n}, \nu)\theta^2 - \tilde{N}_\nu(\mathbf{n})^2, \quad (14b)$$

where

$$p(\theta|\mathbf{n}, \nu) \propto \int_{\varphi_{\min}}^{\varphi_{\max}} d\varphi p(\varphi, \theta) \prod_{i=1}^k p(n_i|\varphi, \theta, \nu_i) \quad (15)$$

is the marginalised posterior. This is our second result.

Eqs. (14) enable optimal atom number sensing. We measure the outcomes $\mathbf{n} = (n_{a,1}, n_{b,1}, \dots, n_{a,k}, n_{b,k})$, with $1 \leq k \leq 30$, alternating photon counts with and without atoms and setting $p(n_i|\varphi, \theta, \nu_i)$ in Eq. (15) for the latter. The frequency is used as an adaptive parameter by optimising the precision gain (6) with $\tilde{\nu}_k(n) \propto \tilde{N}_{\nu_k}(n)$, finding the frequencies $\nu = (\nu_{1a}, \nu_{1b}, \dots, \nu_{ka}, \nu_{kb})$. We choose $p(\varphi, \theta) = p_{\text{MI}}(\varphi, \theta)$ with $5 \leq \varphi \leq 20$ and $0 \leq \theta \leq 8$. For the Cs D₂ $F = 4 \rightarrow F' = 5$ transition, $\nu_r = 351.721961$ THz, $\Gamma = 2\pi \cdot 5.234$ MHz, and in this system of π -polarised light imaging atoms in a fibre junction $\kappa = 84.9$ [47, 63]. Eqs. (6) and (14) are rapidly evaluated between shots by caching function results, managing tolerances, and adaptively truncating probabilities; see the Supplemental Material.

To quantify the effectiveness of this adaptive, symmetry-informed Bayesian strategy, we compare it to four methods previously employed. The standard method uses light resonant with the atomic transition and yields optical depth—thus

| | On resonance | On resonance Detuned | On resonance Bayesian | <i>A priori</i> Bayesian | Adaptive Bayesian |
|------------|--------------|----------------------|-----------------------|--------------------------|-------------------|
| NSR in % | 0.89 | 6.10 | 0.62 | 0.77 | 0.19 |
| k_{\min} | 13 | 17 | 12 | 12 | 8 |

Table I. Comparison of atom number estimation strategies in terms of noise-to-signal ratio for $k = 30$ measurement shots, as well as minimal number of shots k_{\min} for which the estimate stays within 10% of the final estimate.

atom number—by equating the transmittance with the ratio of empirical mean photon counts with and without atoms: $\exp(-\zeta_\nu \Theta) = \langle n_a \rangle / \langle n_b \rangle$ [47], with error propagated from this formula. The second method is analogous, but with frequency detuned $\nu - \nu_r = 5$ MHz below the atomic resonance. The third method employs the resonance frequency, as before, but using the Bayesian estimator in Eqs. (14). The fourth method is as the previous one, but using light at the frequency maximising the precision gain (6) for $k = 1$; this is an *a priori* optimisation as it involves no outcomes [23, 35]. The last two methods use the same prior as the adaptive approach. All other parameters are identical for the five methods.

Results.—Fig. 2 shows the atom number estimates yielded by the on-resonance (blue inverted triangles), detuned (orange triangles), on-resonance Bayesian (red squares), *a priori* Bayesian (purple rhombuses), and adaptive Bayesian (green circles) strategies. We repeat each strategy m times and quantify its performance by the empirical noise-to-signal ratio (NSR) $\text{Var}(\tilde{N}_k) / \langle \tilde{N}_k \rangle^2$ [35], where

$$\text{Var}(\tilde{N}_k) = \langle \tilde{N}_k^2 \rangle - \langle \tilde{N}_k \rangle^2, \quad \text{with} \quad \langle \tilde{N}_k \rangle = \frac{1}{m} \sum_{j=1}^m \tilde{N}_{k,j}, \quad (16)$$

and the k -th estimate during the j -th repetition is denoted as $\tilde{N}_{k,j}$. The results, given in Tab. I, clearly show that the different strategies exhibit marked differences in their performance. While the two non-adaptive Bayesian strategies yield a NSR comparable to that for the on-resonance approach, just under 1%, and all three outperform the detuned strategy by an order of magnitude, the adaptive strategy surpasses them all with a NSR of less than 0.2%. Notably, the latter outperforms the on-resonance approach—which, we recall, is the current standard for cold atom platforms—by a factor of 4.68. This approximately five-fold enhancement constitutes our third result.

Fig. 3 shows that these conclusions hold even for a low shot number. There, the aforementioned NSR is represented as a function of k . A crucial implication is that the NSR achieved by the standard technique (blue inverted triangles) using $k = 30$ shots is rendered by the adaptive strategy (green circles) with only $k = 9$ shots, i.e., about third of the resources. This is our fourth result. Interestingly, Fig. 3 also shows that the *a priori* strategy (purple rhombuses), while simpler to implement, can be notably worse than an adaptive treatment despite already benefiting from use of the precision gain (6), which had been predicted in Ref. [35].

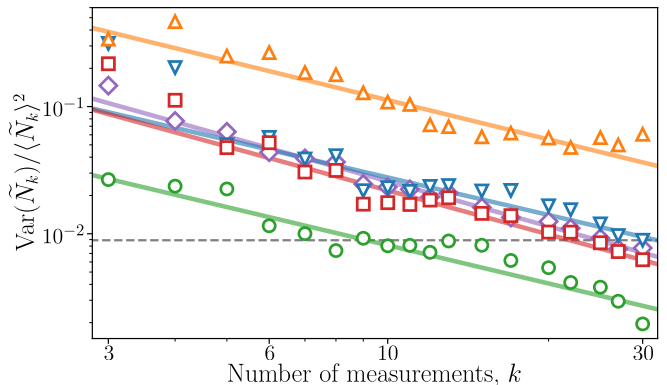


Figure 3. Noise-to-signal ratio (NSR) versus shot number k for the on-resonance (blue inverted triangles), detuned (orange triangles), on-resonance Bayesian (red squares), *a priori* Bayesian (purple rhombuses), and adaptive Bayesian (green circles) strategies. This is obtained empirically from the distribution of m estimates after each shot number k . Solid lines correspond to a power law fit to guide the eye. The dashed line shows that the NSR for on-resonance strategy with 30 shots is achieved by the adaptive strategy with only 9 shots.

The adaptive strategy was also found to converge to a final result within a desired precision faster. We recorded the number of measurement steps k_{\min} needed before the current estimate settled within 10% of the final estimate based on 30 shots, with results shown in the last row of Tab. I. As can be seen, the adaptive method achieves the specified fractional precision with approximately 40% fewer shots than the standard on-resonance strategy requires. This is our final result.

Conclusions.—This Letter demonstrates significantly enhanced atom number sensing in a cold atom platform using adaptive Bayesian techniques. It represents a five-fold increase in precision compared to current standards and a 40% reduction in the number of shots required for estimator convergence. It further shows that real-time adaptive optimisation is feasible with standard computational resources even in multiparameter setups [24, 35]. Overall, the symmetry-informed framework in Eqs. (3) and (6) enables accelerated data collection across the quantum technology sector, expanding beyond the application range of Bayesian phase estimation [64] and easing further adoption of Bayesian techniques.

An immediate application in absorption imaging and spectroscopy is to adaptively optimise optical power or exposure duration; due to the saturable nature of atomic absorbers, there is always a non-trivial optimum for these parameters. At a fundamental level, the next step is implementing not only optimal estimators, but also optimal states $\rho_y(\theta)$ and measurements $\mathcal{M}_y(n)$ with statistics $p(n|\theta, y) = \text{Tr}[\mathcal{M}_y(n)\rho_y(\theta)]$; optimal measurements are given by projecting onto the eigenspace of an operator $\mathcal{S}_{y,f}$ solution to the Lyapunov equation

$$\mathcal{S}_{y,f} \rho_{y,f,0} + \rho_{y,f,0} \mathcal{S}_{y,f} = 2\rho_{y,f,1}, \quad (17)$$

with $\rho_{y,f,l} = \int d\theta p(\theta) \rho_y(\theta) f(\theta)^l$ [46, 65], while optimal states can be found by combining this with techniques such as tensor networks and machine learning [45, 66–71].

Acknowledgments.—JR gratefully thanks J. Boeyens, J. Glatthard, G. Barontini, V. Guarrera, M. Tsang and L. Correa for helpful discussions, and acknowledges financial support from the Surrey Future Fellowship Programme. JA gratefully acknowledges funding from EPSRC (EP/R045577/1) and thanks the Royal Society for support. The experiment was supported by the grant 62420 from the John Templeton Foundation, the IUK project No.133086, EPSRC grants EP/T001046/1, EP/R024111/1, EP/M013294/1, EP/Y005139/1 and EP/Z533166/1, and by the European Commission grant ErBeStA (no.800942).

Data availability.—All data upon which our conclusions are based are presented herein. All additional data related to the experimental system are available from the authors upon reasonable request.

For the purpose of open access, the authors have applied a 'Creative Commons Attribution' (CC BY) licence to any Author Accepted Manuscript version arising from this submission.

* The first two authors contributed equally to this work. Corresponding author: j.rubiojimenez@surrey.ac.uk

- [1] J. M. Hogan and M. A. Kasevich, Atom-interferometric gravitational-wave detection using heterodyne laser links, *Phys. Rev. A* **94**, 033632 (2016).
- [2] L. Badurina, E. Bentine, D. Blas, K. Bongs, D. Bortoletto, T. Bowcock, K. Bridges, W. Bowden, O. Buchmueller, C. Burrage, J. Coleman, G. Elertas, J. Ellis, C. Foot, V. Gibson, M. Haehnel, T. Harte, S. Hedges, R. Hobson, M. Holynski, T. Jones, M. Langlois, S. Lellouch, M. Lewicki, R. Maiolino, P. Majewski, S. Malik, J. March-Russell, C. McCabe, D. Newbold, B. Sauer, U. Schneider, I. Shipsey, Y. Singh, M. Uchida, T. Valenzuela, M. v. d. Grinten, V. Vaskonen, J. Vossebel, D. Weatherill, and I. Wilmut, Aion: an atom interferometer observatory and network, *J. Cosmol. Astropart. Phys.* **2020** (05), 011–011.
- [3] R. Zhang, W. Xiao, Y. Ding, Y. Feng, X. Peng, L. Shen, C. Sun, T. Wu, Y. Wu, Y. Yang, Z. Zheng, X. Zhang, J. Chen, and H. Guo, Recording brain activities in unshielded earth's field with optically pumped atomic magnetometers, *Sci. Adv.* **6**, eaba8792 (2020).
- [4] C. L. Degen, F. Reinhard, and P. Cappellaro, Quantum sensing, *Rev. Mod. Phys.* **89**, 035002 (2017).
- [5] E. Boto, N. Holmes, J. Leggett, G. Roberts, V. Shah, S. S. Meyer, L. D. Muñoz, K. J. Mullinger, T. M. Tierney, S. Bestmann, G. R. Barnes, R. Bowtell, and M. J. Brookes, Moving magnetoencephalography towards real-world applications with a wearable system., *Nature* **555**, 657–66 (2018).
- [6] F. A. Narducci, A. T. Black, and J. H. Burke, Advances toward fieldable atom interferometers, *Adv. Phys. X* **7**, 1946426 (2022).
- [7] J. Lee, R. Ding, J. Christensen, R. R. Rosenthal, A. Ison, D. P. Gillund, D. Bossert, K. H. Fuerschbach, W. Kindel, P. S. Finnegan, J. R. Wendt, M. Gehl, A. Kodigala, H. McGuinness, C. A. Walker, S. A. Kemme, A. Lentine, G. Biedermann, and P. D. D. Schwindt, A compact cold-atom interferometer with a high data-rate grating magneto-optical trap and a photonic-integrated-circuit-compatible laser system, *Nat. Commun.* **13**, 5131 (2022).
- [8] B. Adams, S. Kinge, K. Bongs, and Y. H. Lien, Magneto-optical trap performance for high-bandwidth applications, *Phys. Rev. A* **108**, 063111 (2023).
- [9] T. M. Graham, Y. Song, J. Scott, C. Poole, L. Phuttitarn, K. Jooya, P. Eichler, X. Jiang, A. Marra, B. Grinkemeyer, M. Kwon, M. Ebert, J. Cherek, M. T. Lichtman, M. Gillette, J. Gilbert, D. Bowman, T. Ballance, C. Campbell, E. D. Dahl, O. Crawford, N. S. Blunt, B. Rogers, T. Noel, and M. Saffman, Multi-qubit entanglement and algorithms on a neutral-atom quantum computer, *Nature* **604**, 457 (2022).
- [10] Wintersperger, Karen, Dommert, Florian, Ehmer, Thomas, Hoursanov, Andrey, Klepsch, Johannes, Mauerer, Wolfgang, Reuber, Georg, Strohm, Thomas, Yin, Ming, and Lubner, Sebastian, Neutral atom quantum computing hardware: performance and end-user perspective, *EPJ Quantum Technol.* **10**, 32 (2023).
- [11] P. Horodecki, L. Rudnicki, and K. Życzkowski, Five open problems in quantum information theory, *PRX Quantum* **3**, 010101 (2022).
- [12] S. G. Turyshev, U. E. Israelsson, M. Shao, N. Yu, A. Kuzenko, E. L. Wright, C. W. F. Everitt, M. Kasevich, J. A. Lipa, J. C. Mester, R. D. Reasenberg, R. L. Walsworth, N. Ashby, H. Gould, and H. J. Paik, Space-based research in fundamental physics and quantum technologies, *Int. J. Mod. Phys. D* **16**, 1879 (2007).
- [13] R. Kaltenbaek, A. Acin, L. Bacsardi, P. Bianco, P. Bouyer, E. Diamanti, C. Marquardt, Y. Omar, V. Pruneri, E. Rasel, *et al.*, Quantum technologies in space, *Exp. Astron.* **51**, 1677 (2021).
- [14] A. Belenchia, M. Carlesso, Ömer Bayraktar, D. Dequal, I. Derkach, G. Gasbarri, W. Herr, Y. L. Li, M. Rademacher, J. Sidhu, D. K. Oi, S. T. Seidel, R. Kaltenbaek, C. Marquardt, H. Ulbricht, V. C. Usenko, L. Wörner, A. Xuereb, M. Paternostro, and A. Bassi, Quantum physics in space, *Phys. Rep.* **951**, 1 (2022).
- [15] J. Ye and P. Zoller, Essay: Quantum sensing with atomic, molecular, and optical platforms for fundamental physics, *Phys. Rev. Lett.* **132**, 190001 (2024).
- [16] S. D. Bass and M. Doser, Quantum sensing for particle physics, *Nat. Rev. Phys.* **6**, 329 (2024).
- [17] S. M. Kay, *Fundamentals of Statistical Signal Processing: Estimation Theory* (Prentice Hall, 1993).
- [18] M. G. Paris, Quantum estimation for quantum technology, *Int. J. Quantum Inf.* **7**, 125 (2009).
- [19] R. Demkowicz-Dobrzański, M. Jarzyna, and J. Kołodyński, Quantum Limits in Optical Interferometry, *Prog. Opt.* **60**, 345 (2015).
- [20] V. Montenegro, C. Mukhopadhyay, R. Yousefjani, S. Sarkar, U. Mishra, M. G. A. Paris, and A. Bayat, *Review: Quantum metrology and sensing with many-body systems*, arXiv:2408.15323 (2024).
- [21] E. T. Jaynes, *Probability Theory: The Logic of Science* (Cambridge University Press, 2003).
- [22] J. Liu, H. Yuan, X.-M. Lu, and X. Wang, Quantum Fisher information matrix and multiparameter estimation, *J. Phys. A: Math. Theor.* **53**, 023001 (2020).
- [23] J. Rubio and J. A. Dunningham, Quantum metrology in the presence of limited data, *New J. Phys.* **21**, 043037 (2019).
- [24] M. Valeri, E. Polino, D. Poderini, I. Gianani, G. Corrielli, A. Crespi, R. Osellame, N. Spagnolo, and F. Sciarrino, Experimental adaptive Bayesian estimation of multiple phases with limited data, *npj Quantum Inf.* **6**, 92 (2020).
- [25] S. Morelli, A. Usui, E. Agudelo, and N. Friis, Bayesian para-

- meter estimation using Gaussian states and measurements, *Quantum Sci. Technol.* **6**, 025018 (2021).
- [26] J. Rubio, J. Anders, and L. A. Correa, Global quantum thermometry, *Phys. Rev. Lett.* **127**, 190402 (2021).
- [27] W. Salmon, S. Strelchuk, and D. Arvidsson-Shukur, Only Classical Parameterised States have Optimal Measurements under Least Squares Loss, *Quantum* **7**, 998 (2023).
- [28] J. J. Meyer, S. Khatiri, D. S. França, J. Eisert, and P. Faist, *Quantum metrology in the finite-sample regime*, arXiv:2307.06370 (2023).
- [29] W. v. d. Linden, V. Dose, and U. v. Toussaint, *Bayesian Probability Theory: Applications in the Physical Sciences* (Cambridge University Press, 2014).
- [30] D. Brivio, S. Cialdi, S. Vezzoli, B. T. Gebrehiwot, M. G. Genoni, S. Olivares, and M. G. A. Paris, Experimental estimation of one-parameter qubit gates in the presence of phase diffusion, *Phys. Rev. A* **81**, 012305 (2010).
- [31] S. Paesani, A. A. Gentile, R. Santagati, J. Wang, N. Wiebe, D. P. Tew, J. L. O'Brien, and M. G. Thompson, Experimental Bayesian Quantum Phase Estimation on a Silicon Photonic Chip, *Phys. Rev. Lett.* **118**, 100503 (2017).
- [32] A. Lumino, E. Polino, A. S. Rab, G. Milani, N. Spagnolo, N. Wiebe, and F. Sciarrino, Experimental phase estimation enhanced by machine learning, *Phys. Rev. Appl.* **10**, 044033 (2018).
- [33] R. Kaubruegger, D. V. Vasilyev, M. Schulte, K. Hammerer, and P. Zoller, Quantum Variational Optimization of Ramsey Interferometry and Atomic Clocks, *Phys. Rev. X* **11**, 041045 (2021).
- [34] I. Gianani, M. G. Genoni, and M. Barbieri, Assessing data post-processing for quantum estimation, *IEEE J. Sel. Top. Quantum Electron.* **26**, 1 (2020).
- [35] J. Glatthard, J. Rubio, R. Sawant, T. Hewitt, G. Barontini, and L. A. Correa, Optimal Cold Atom Thermometry Using Adaptive Bayesian Strategies, *PRX Quantum* **3**, 040330 (2022).
- [36] L. Gerster, F. Martínez-García, P. Hrmo, M. W. van Mourik, B. Wilhelm, D. Vodola, M. Müller, R. Blatt, P. Schindler, and T. Monz, Experimental Bayesian Calibration of Trapped-Ion Entangling Operations, *PRX Quantum* **3**, 020350 (2022).
- [37] M. Valeri, V. Cimini, S. Piacentini, F. Ceccarelli, E. Polino, F. Hoch, G. Bizzarri, G. Corrielli, N. Spagnolo, R. Osellame, and F. Sciarrino, Experimental multiparameter quantum metrology in adaptive regime, *Phys. Rev. Res.* **5**, 013138 (2023).
- [38] A. Oliveira, J. Rubio, C. Noble, J. Anderson, J. Anders, and A. Mulholland, Fluctuation relations to calculate protein redox potentials from molecular dynamics simulations, *J. Chem. Theory Comput.* **20**, 385 (2023).
- [39] V. Cimini, E. Polino, M. Valeri, N. Spagnolo, and F. Sciarrino, Benchmarking Bayesian quantum estimation, *Quantum Sci. Technol.* **9**, 035035 (2024).
- [40] F. Belliardo, V. Cimini, E. Polino, F. Hoch, B. Piccirillo, N. Spagnolo, V. Giovannetti, and F. Sciarrino, Optimizing quantum-enhanced Bayesian multiparameter estimation of phase and noise in practical sensors, *Phys. Rev. Res.* **6**, 023201 (2024).
- [41] T. Hewitt, T. Bertheas, M. Jain, Y. Nishida, and G. Barontini, Controlling the interactions in a cold atom quantum impurity system, *Quantum Sci. Technol.* **9**, 035039 (2024).
- [42] C. W. Helstrom, *Quantum Detection and Estimation Theory* (Academic Press, New York, 1976).
- [43] G. D'Agostini, Bayesian inference in processing experimental data: principles and basic applications, *Rep. Prog. Phys.* **66**, 1383 (2003).
- [44] R. Demkowicz-Dobrzański, W. Górecki, and M. Guță, Multiparameter estimation beyond quantum Fisher information, *J. Phys. A: Math. Theor.* **53**, 363001 (2020).
- [45] J. Bavaresco, P. Lipka-Bartosik, P. Sekatski, and M. Mehboudi, Designing optimal protocols in Bayesian quantum parameter estimation with higher-order operations, *Phys. Rev. Res.* **6**, 023305 (2024).
- [46] J. Rubio, First-principles construction of symmetry-informed quantum metrologies, *Phys. Rev. A* **110**, L030401 (2024).
- [47] E. D. Ros, N. Cooper, J. Nute, and L. Hackermueller, Cold atoms in micromachined waveguides: A new platform for atom-photon interactions, *Phys. Rev. Research* **2**, 033098 (2020).
- [48] E. Polino, M. Valeri, N. Spagnolo, and F. Sciarrino, Photonic quantum metrology, *AVS Quantum Science* **2**, 024703 (2020).
- [49] M. Mehboudi, M. R. Jørgensen, S. Seah, J. B. Brask, J. Kołodyński, and M. Perarnau-Llobet, Fundamental Limits in Bayesian Thermometry and Attainability via Adaptive Strategies, *Phys. Rev. Lett.* **128**, 130502 (2022).
- [50] S. Kurdziałek, W. Górecki, F. Albarelli, and R. Demkowicz-Dobrzański, Using adaptiveness and causal superpositions against noise in quantum metrology, *Phys. Rev. Lett.* **131**, 090801 (2023).
- [51] J. G. Smith, C. H. W. Barnes, and D. R. M. Arvidsson-Shukur, Adaptive Bayesian quantum algorithm for phase estimation, *Phys. Rev. A* **109**, 042412 (2024).
- [52] N. Cooper, E. D. Ros, C. Briddon, V. Naniyil, M. Greenaway, and L. Hackermueller, Prospects for strongly coupled atom-photon quantum nodes, *Sci. Rep.* **9**, 7798 (2019).
- [53] W. Bogaerts, D. Pérez, J. Capmany, D. A. B. Miller, J. Poon, D. Englund, F. Morichetti, and A. Melloni, Programmable photonic circuits, *Nature* **586**, 207 (2020).
- [54] B. MacLellan, P. Roztocky, S. Czischek, and R. G. Melko, *End-to-end variational quantum sensing*, arXiv:2403.02394 (2024).
- [55] R. E. Kass and L. Wasserman, The Selection of Prior Distributions by Formal Rules, *J Am Stat Assoc* **91**, 1343 (1996).
- [56] J. Rubio, Quantum scale estimation, *Quantum Sci. Technol.* **8**, 015009 (2022).
- [57] T. Nieddu, V. Gokhroo, and S. N. Chormaic, Optical nanofibres and neutral atoms, *Journal of Optics* **18** (2016).
- [58] C.-B. Zhang, D.-Q. Su, Z.-H. Ji, Y.-T. Zhao, L.-T. Xiao, and S.-T. Jia, Measurement of Zeeman shift of Cesium atoms using an optical nanofiber, *Chinese Phys. Lett.* **35**, 083201 (2018).
- [59] C. Troullinou, V. G. Lucivero, and M. W. Mitchell, Quantum-enhanced magnetometry at optimal number density, *Phys. Rev. Lett.* **131**, 133602 (2023).
- [60] Z. Zhou, S. C. Carrasco, C. Sanner, V. S. Malinovsky, and R. Folman, Geometric phase amplification in a clock interferometer for enhanced metrology, arXiv: , 2405.10226 (2024).
- [61] T. J. Proctor, P. A. Knott, and J. A. Dunningham, Multiparameter estimation in networked quantum sensors, *Phys. Rev. Lett.* **120**, 080501 (2018).
- [62] J. Rubio, P. A. Knott, T. J. Proctor, and J. A. Dunningham, Quantum sensing networks for the estimation of linear functions, *J. Phys. A: Math. Theor.* **53**, 344001 (2020).
- [63] D. A. Steck, Cesium D line data, revision 2.3.3, <http://steck.us/alkalidata> (2024), accessed: 2024-09-10.
- [64] R. Demkowicz-Dobrzański, Optimal phase estimation with arbitrary a priori knowledge, *Phys. Rev. A* **83**, 061802 (2011).
- [65] M. Tsang, Generalized conditional expectations for quantum retrodiction and smoothing, *Phys. Rev. A* **105**, 042213 (2022).
- [66] I. S. M. Schuld and F. Petruccione, An introduction to quantum machine learning, *Contemp. Phys.* **56**, 172 (2015).
- [67] L. J. Fiderer, J. Schuff, and D. Braun, Neural-Network Heuristics for Adaptive Bayesian Quantum Estimation, *PRX Quantum* **2**, 020303 (2021).

- [68] D. Koutný, L. Motka, Z. c. v. Hradil, J. Řeháček, and L. L. Sánchez-Soto, Neural-network quantum state tomography, *Phys. Rev. A* **106**, 012409 (2022).
- [69] V. Gebhart, R. Santagati, A. A. Gentile, E. M. Gauger, D. Craig, N. Ares, L. Bianchi, F. Marquardt, L. Pezzè, and C. Bonato, Learning quantum systems, *Nat. Rev. Phys.* **5**, 141 (2023).
- [70] E. Rinaldi, M. G. Lastre, S. G. Herreros, S. Ahmed, M. Khanahmadi, F. Nori, and C. S. Muñoz, Parameter estimation from quantum-jump data using neural networks, *Quantum Sci. Technol.* **9**, 035018 (2024).
- [71] S. Kurdzialek, P. Dulian, J. Majsak, S. Chakraborty, and R. Demkowicz-Dobrzanski, Quantum metrology using quantum combs and tensor network formalism, arXiv:2403.04854 (2024).
- [72] K. F. Riley, M. P. Hobson, and S. J. Bence, *Mathematical Methods for Physics and Engineering*, 3rd ed. (Cambridge University Press, Cambridge, 2006).
- [73] M. Tsang, Operational meanings of a generalized conditional expectation in quantum metrology, *Quantum* **7**, 1162 (2023).
- [74] B. R. Mollow, Stimulated emission and absorption near resonance for driven systems, *Phys. Rev. A* **5**, 2217 (1972).
- [75] W. Guerin, F. Michaud, and R. Kaiser, Mechanisms for lasing with cold atoms as the gain medium, *Phys. Rev. Lett.* **101**, 093002 (2008).
- [76] C. Sayrin, C. Clausen, B. Albrecht, P. Schneeweiss, and A. Rauschenbeutel, Storage of fiber-guided light in a nanofiber-trapped ensemble of cold atoms, *Optica* **2**, 353 (2015).

Supplemental material

The theory underpinning experimental symmetry-informed estimation is presented, and the equations leading to a symmetry function relevant for the cold atom platform employed in this work are solved. Additional experimental data is presented that helps to place the primary results into context and provides an illustrative example of how the optimised Bayesian measurement strategy operates in practice. A brief discussion of efficient numerical evaluation of the optimal probe laser frequency is also provided.

BAYESIAN INFERENCE WITH INCORPORATED SYMMETRIES

Minimal information loss

A flexible approach to designing estimation strategies is minimising an information loss quantifier [21, 42]. Let $\mathcal{L}(\tilde{\theta}, \theta)$ quantify the loss incurred by an estimate $\tilde{\theta}$ should the hypothesis θ be correct. The average loss is defined as

$$\bar{\mathcal{L}}_{\mathbf{y}} = \int d\mathbf{n} p(\mathbf{n}|\mathbf{y}) \mathcal{L}_{\mathbf{y}}(\mathbf{n}), \quad (\text{S1})$$

where $p(\mathbf{n}|\mathbf{y}) = \int d\theta p(\theta) p(\mathbf{n}|\theta, \mathbf{y})$ is the evidence;

$$\mathcal{L}_{\mathbf{y}}(\mathbf{n}) = \int d\theta p(\theta|\mathbf{n}, \mathbf{y}) \mathcal{L}[\tilde{\theta}_{\mathbf{y}}(\mathbf{n}), \theta] \quad (\text{S2})$$

is the loss associated with the vector of outcomes \mathbf{n} , based on the posterior $p(\theta|\mathbf{n}, \mathbf{y})$; \mathbf{y} is a vector of control parameters; and $\tilde{\theta}_{\mathbf{y}}(\mathbf{n})$ is an estimator function, whose form we need to decide.

To do so, we minimise Eq. (S1) with respect to $\tilde{\theta}_{\mathbf{y}}(\mathbf{n})$ using variational calculus. This identifies the *optimal* estimator $\tilde{\vartheta}_{\mathbf{y}}(\mathbf{n})$, in the sense of leading to minimal information loss, as solution to [21, 72]

$$\int d\theta p(\theta|\mathbf{n}, \mathbf{y}) \partial_z \mathcal{L}(z, \theta)|_{z=\tilde{\vartheta}_{\mathbf{y}}(\mathbf{n})} = 0. \quad (\text{S3})$$

Eq. (S3) offers a systematic way of finding good estimation strategies.

Optimal estimators

To solve Eq. (S3), a loss function \mathcal{L} must be chosen. Phase estimation, for instance, deals with circular parameters and so it requires trigonometric losses such as $\mathcal{L}(\tilde{\theta}, \theta) = 4 \sin^2[(\tilde{\theta} - \theta)/2]$ [64]. For parameters other than phases, the quadratic loss

$$\mathcal{L}(\tilde{\theta}, \theta) = [f(\tilde{\theta}) - f(\theta)]^2 \quad (\text{S4})$$

can account for errors in a wide range of information-theoretic scenarios [65, 73]. Here, f is a free function that we use to map the hypothesis θ into a location (or shift) hypothesis $f(\theta)$ [46], in the sense that the aforementioned \mathcal{L} is invariant under translations

$$f(\theta') = f(\theta) + c, \quad (\text{S5})$$

with arbitrary constant c [21, 29]. Those parameters for which f exists can thus be referred to as location-isomorphic [46]. This allows Eq. (S3) to be straightforwardly solved for the estimator function, finding

$$\tilde{\vartheta}_{\mathbf{y},f}(\mathbf{n}) = f^{-1} \left[\int d\theta p(\theta|\mathbf{n}, \mathbf{y}) f(\theta) \right], \quad (\text{S6})$$

as stated in the main text. Under the quadratic loss criterion (S4), this estimator is optimal for any parameter range, sample size, prior, and likelihood function.

Three instances of this formalism have so far been considered in the literature. When $f(z) = z$, Eq. (S5) renders the translation

$$\theta' = \theta + c \quad (\text{S7})$$

and Eq. (S6) becomes

$$\tilde{\vartheta}_{\mathbf{y}}(\mathbf{n}) = \int d\theta p(\theta|\mathbf{n}, \mathbf{y}) \theta, \quad (\text{S8})$$

which is the posterior mean typically employed in location estimation [21, 29]. When $f(z) = \log(z/\theta_0)$, with arbitrary positive constant θ_0 , Eq. (S5) renders the scale transformation

$$\theta' = \gamma\theta, \quad (\text{S9})$$

with $\gamma = \exp(c)$, and Eq. (S6) becomes

$$\tilde{\vartheta}_{\mathbf{y}}(\mathbf{n}) = \theta_0 \exp \left[\int d\theta p(\theta|\mathbf{n}, \mathbf{y}) \log \left(\frac{\theta}{\theta_0} \right) \right], \quad (\text{S10})$$

where θ_0 enforces dimension neutralisation without affecting the value of $\tilde{\vartheta}_{\mathbf{y}}(\mathbf{n})$. This estimator is optimal for scale metrology in general [56], and for global thermometry in particular [26, 49]. Finally, $f(z) = 2\text{artanh}(2z - 1)$ transforms Eq. (S5) into the Möbius transformation

$$\theta' = \frac{\gamma\theta}{1 - \theta + \gamma\theta}, \quad (\text{S11})$$

with the same γ as before, and Eq. (S6) into

$$\tilde{\vartheta}_{\mathbf{y}}(\mathbf{n}) = \frac{1}{2} + \frac{1}{2} \tanh \left[\int d\theta p(\theta|\mathbf{n}, \mathbf{y}) \text{artanh}(2\theta - 1) \right], \quad (\text{S12})$$

which enables the optimal estimation of weight parameters [46]. Devising a good estimation strategy for quantum technology platforms using this method amounts to identifying a suitable function f .

Information loss and error bars

Inserting Eqs. (S4) and (S6) into Eq. (S2) further leads to the average loss incurred by postprocessing the outcomes \mathbf{n} with the optimal strategy:

$$\mathcal{L}_{\mathbf{y},f}(\mathbf{n}) = \int d\theta p(\theta|\mathbf{n}, \mathbf{y}) f(\theta)^2 - f[\tilde{\vartheta}_{\mathbf{y},f}(\mathbf{n})]^2. \quad (\text{S13})$$

The resulting pair $(\tilde{\vartheta}_{\mathbf{y},f}(\mathbf{n}), \mathcal{L}_{\mathbf{y},f}(\mathbf{n}))$ suffices to report and compare estimates for given f . However, to facilitate the visualisation of the quality of our estimates, it is useful to also construct a Bayesian analogue of error bars.

Let us first note that, when $\tilde{\theta} \approx \theta$, the quadratic loss (S4) can be Taylor-expanded as

$$\mathcal{L}(\tilde{\theta}, \theta) \approx f'(\theta)^2 (\tilde{\theta} - \theta)^2, \quad (\text{S14})$$

which is the familiar square error multiplied by a factor of $f'(\theta)^2$. Given this, we now *define* the error bar associated with the optimal estimator (S6) as

$$\Delta \tilde{\vartheta}_{\mathbf{y},f}(\mathbf{n}) := \frac{\sqrt{\mathcal{L}_{\mathbf{y},f}(\mathbf{n})}}{|f'[\tilde{\vartheta}_{\mathbf{y},f}(\mathbf{n})]|}. \quad (\text{S15})$$

This is a symmetry-informed analogue of the standard deviation, which guarantees dimensional consistency between estimates and errors. As such, we can use $\hat{v}_{\mathbf{y},f}(\mathbf{n}) \pm \Delta \hat{v}_{\mathbf{y},f}(\mathbf{n})$ to report the results.

Strictly speaking, error bars are most naturally suited for the estimation of location parameters in Gaussian-like distributions. For any other scenario, error bars are a useful heuristic at best, and they tend to be less reliable in regimes with limited data. While this sometimes goes unnoticed, Eq. (S15) brings this local nature to light by virtue of being motivated by the local approximation in Eq. (S14), which only holds for either narrow hypothesis ranges or asymptotically large data sets. Despite this, we choose to represent our Bayesian errors in this way for consistency with current practice. Note that this does not negate the general validity of the average loss (S13).

Symmetry function for our platform from a multiparameter ignorance prior

We now focus on identifying f . In the main text, the transformation

$$\varphi' = \gamma\varphi, \quad \zeta_\nu\theta' = \zeta_\nu\theta + \log(\gamma), \quad (\text{S16})$$

with arbitrary positive constant γ , is identified as a key invariance enabling a meaningful notion of maximum ignorance in our platform. This is represented by a prior $p_{\text{MI}}(\varphi, \theta|\nu)$ satisfying two conditions:

1. invariance under Eq. (S16), i.e., $p_{\text{MI}}(\varphi', \theta'|\nu)d\varphi'd\theta' = p_{\text{MI}}(\varphi, \theta|\nu)d\varphi d\theta$;
2. ν does not inform the value of the unknown parameters.

We recall that φ and θ denote hypotheses for the expected photon number without atoms present and the on-resonance optical depth, respectively, while ν is the laser frequency playing the role of a control parameter.

Condition 1 implies the functional equation

$$\gamma p_{\text{MI}} \left[\gamma\varphi, \theta + \frac{\log(\gamma)}{\zeta_\nu} \middle| \nu \right] = p_{\text{MI}}(\varphi, \theta|\nu). \quad (\text{S17})$$

By taking the derivative with respect to γ on both sides, we can transform it into the partial differential equation

$$\zeta_\nu p_{\text{MI}}(x, y|\nu) + \zeta_\nu x \partial_x p_{\text{MI}}(x, y|\nu) + \partial_y p_{\text{MI}}(x, y|\nu) = 0. \quad (\text{S18})$$

Solving for $p_{\text{MI}}(x, y|\nu)$, we find

$$p_{\text{MI}}(\varphi, \theta|\nu) = e^{-\zeta_\nu\theta} h(\varphi e^{-\zeta_\nu\theta}), \quad (\text{S19})$$

where h is an arbitrary function. As such, and unlike in many single-parameter scenarios [21, 29], condition 1 does not fully determine the ignorance prior we seek.

Condition 2, which allows us to drop the dependency of the prior on the laser frequency as $p_{\text{MI}}(\varphi, \theta|\nu) \rightarrow p_{\text{MI}}(\varphi, \theta)$ [21], suffices to address this problem. This condition is already satisfied for $\theta = 0$, since $p_{\text{MI}}(\varphi, 0) = h(\varphi)$. For $\theta \neq 0$, we can enforce the aforementioned independence by setting the derivative of Eq. (S19) with respect to ν to zero. Provided that $\nu \neq \nu_r$, so that $d\zeta_\nu/d\nu \neq 0$, we find

$$h(z) + z h'(z) = 0, \quad (\text{S20})$$

whose solution is $h(z) \propto 1/z$. Therefore, the prior representing maximum ignorance about the unknown parameters of our cold atom platform is

$$p_{\text{MI}}(\varphi, \theta) \propto \frac{1}{\varphi}. \quad (\text{S21})$$

The prior in the main text is recovered by normalising Eq. (S21) over the range $[\varphi_{\min}, \varphi_{\max}] \times [\theta_{\min}, \theta_{\max}]$.

Since φ is a nuisance parameter, the final step is marginalising Eq. (S21) over it, i.e.,

$$p_{\text{MI}}(\theta) = \int_{\varphi_{\min}}^{\varphi_{\max}} d\varphi p_{\text{MI}}(\varphi, \theta) \propto 1, \quad (\text{S22})$$

and equating the result to $p_{\text{MI}}(\theta) \propto f'(\theta)$. This leads to $f'(z) \propto 1$, whose solution is

$$f(z) = c_1 z + c_2. \quad (\text{S23})$$

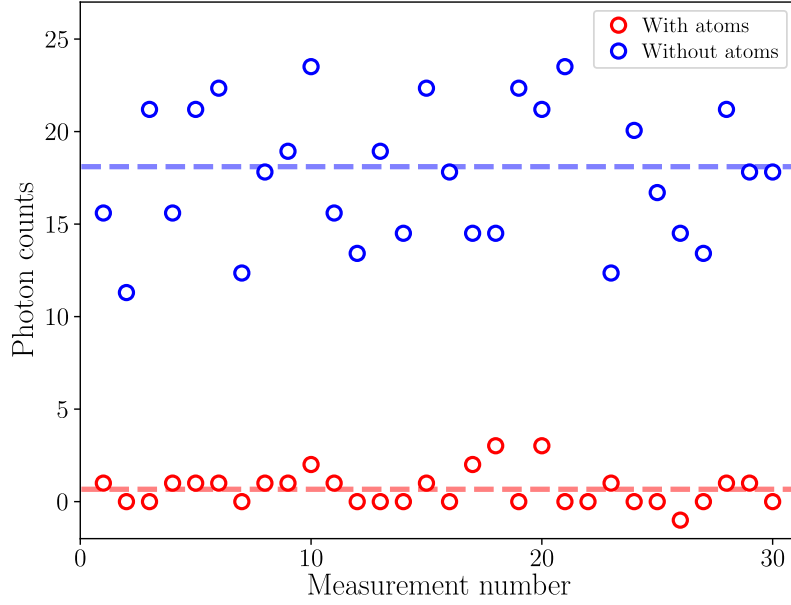


Figure S1. Example of an experimental run consisting of 30 measurements, with atoms present in the hole (red circles) and without (blue circles), using resonant light.

This is the *symmetry function* for our setup. We choose $c_1 = 1$ in order to render the familiar square loss $\mathcal{L}(\tilde{\theta}, \theta) = (\tilde{\theta} - \theta)^2$ and $c_2 = 0$ without loss of generality, so that $f(z) = z$.

Once derived, this result may appear straightforward. However, the method laid out above provides a systematic approach to determining the form of $f(z)$ for any platform, including potentially complex multiparameter setups, as is the case for us. In addition, we note that this symmetry leads to an optimal estimator for the on-resonance optical depth as in Eq. (S8), which can take negative values. These correspond to amplifying atomic media, for example as described in [74, 75], and they occur only in conjunction with negative κ , so that atom number estimates $\tilde{N}_\nu(\mathbf{n}) = \kappa \tilde{\nu}_\nu(\mathbf{n})$ are always positive.

MEASUREMENT OF ATOM NUMBER IN A COLD ATOM PLATFORM

Fig. S1 shows an example of a sample with ~ 250 atoms and a measurement run taken with resonant light of frequency ν_r , consisting of $k = 30$ shots with atoms (red circles), $\mathbf{n}_a = (n_{a,1}, \dots, n_{a,k})$, and $l = 30$ shots without atoms (blue circles), $\mathbf{n}_b = (n_{b,1}, \dots, n_{b,l})$. For each data point, atoms are cooled in a magneto-optical trap, transferred to an optical dipole trap and positioned in the intersection of the optical fibre. The atoms are held in the fibre junction for 5 ms before they are imaged using a $10 \mu\text{s}$ imaging pulse sent through the optical fibre and detected at a single photon counting module (SPCM). A detector dark count rate of $n \sim 1$ is measured independently and subtracted from both signals.

Constraints

The photon counts recorded in each case will be Poisson-distributed about their mean value. The small mode area of the intersection ($\sim 20 \mu\text{m}^2$) together with the saturability of the atomic medium limits the applied optical power to $\sim \text{pW}$, while expansion of the atomic cloud restricts the exposure duration. Total photon counts are thus limited to a few tens of photons per measurement step, which is how photon-counting statistics become the limiting factor on measurement precision. Typically, 30 - 100 measurement steps are required for atom number estimation, each taking approximately 6 s. These requirements are comparable to, e.g., Refs. [59] and [76].

For the example in Fig. S1, $k = 30$ measurements are taken using resonant light with empirical means $\langle n_a \rangle = 0.7 \pm 0.2$ and $\langle n_b \rangle = 18.1 \pm 0.8$. When analysed using the standard method, this leads to an atom number estimate of $\tilde{N}_k = 283 \pm 22$. When analysed using the Bayesian method (red squares in Figs. 2 and 3, Eqs. (14) in the main text), it gives an atom number of $\tilde{N}_k = 277 \pm 19$. Since these example data were collected with the frequency fixed on resonance, the other methods do not apply. (Tab. S1 expands the results for all methods in the main text.)

| | m | $\langle \tilde{N}_k \rangle$ | $[\text{Var}(\tilde{N}_k)]^{\frac{1}{2}}$ | $\text{Var}(\tilde{N}_k)/\langle \tilde{N}_k^2 \rangle$ | $\langle \Delta \tilde{N}_k \rangle$ |
|--------------------------|-----|-------------------------------|---|---|--------------------------------------|
| On resonance | 16 | 279 | 26 | 0.89 % | 27 |
| Detuned | 12 | 313 | 77 | 6.10 % | 47 |
| On resonance Bayesian | 16 | 268 | 21 | 0.62 % | 19 |
| <i>A priori</i> Bayesian | 19 | 238 | 21 | 0.77 % | 16 |
| Adaptive Bayesian | 16 | 258 | 11 | 0.19 % | 18 |

Table S1. Overview of parameters of Fig. 2 in the main text, including: number of repeats m ; mean of the individual estimates, $\langle \tilde{N}_k \rangle$; the correspondent standard deviation, $[\text{Var}(\tilde{N}_k)]^{\frac{1}{2}}$; empirical noise-to-signal ratio; and mean of the individual error bars of each estimate \tilde{N}_k from m repeats, $\langle \Delta \tilde{N}_k \rangle$.

Experimental implementation of the adaptive Bayesian protocol

To implement the adaptive Bayesian method, the precision gain quantifier in Eq. (6), \mathcal{G}_{ν_k} , needs be maximised and the optimal frequency calculated in real time and adapted physically sufficiently fast between the measurement shots with an experimental run time of 6 s. This can be achieved in Python 3 on a standard desktop computer. Standard techniques, such as caching of function outputs, control of error tolerances and interpolation were employed to reduce evaluation time. In addition, adaptive truncation of the probability distributions for θ , \bar{n}_b and n (the on-resonance optical depth hypothesis, expected photon counts without atoms and photon counts recorded from a specific shot, respectively) was used. The truncation ranges were set such that, using the posterior probability distribution in light of all previous measurements, we integrated only over regions where the probability densities were greater than 1 % of their maximum values, with sums over possible n truncated at the same probability threshold, but under the worst-case assumption for θ and \bar{n}_b , i.e., the sum was only truncated once this threshold was passed for all possible values of θ and \bar{n}_b remaining within the truncation window.

The laser frequency was adjusted via a voltage-controlled oscillator within an optical beat lock that stabilises the laser frequency. An example of how the gain function and hence optimal laser frequency changes over the course of a measurement run when the adaptive protocol is applied is shown in figure S2.

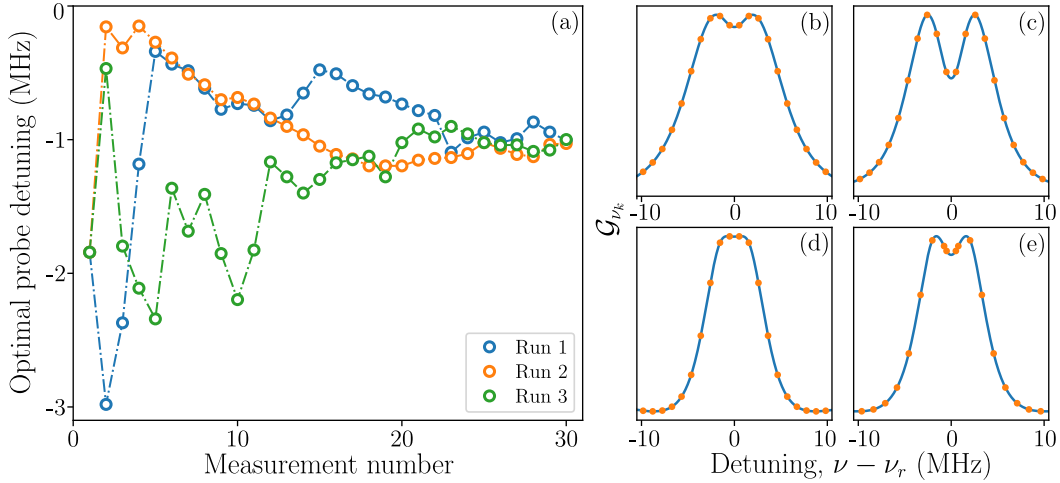


Figure S2. (a) Example of how the optimal measurement frequency ν changes when the adaptive Bayesian feedback is applied. Three consecutive experimental runs are shown, where the sample has been prepared with an atom number of $N \sim 250$. (b-e) Examples of the gain function \mathcal{G}_{ν_k} used to find the optimal frequency [Eq. (6)]. Examples are shown for: (b) the *a priori* case, $k = 1$; (c) high current atom number estimate, $N \sim 340$ $k = 4$; (d) low current atom number estimate, $N \sim 200$ $k = 4$; (e) at the end of a run, $N \sim 250$ $k = 30$. Orange dots show the calculated values, while the blue line is a cubic interpolation.